Supporting Information

Pyridinic-Nitrogen-Highly Doping Nanotubular Carbon Arrays Grown on Carbon Cloth for High Performance and Flexible Supercapacitors

Rui Li,[a,+] Xiaodong Li,[a,+] Jin Chen,[a] Jun Wang,[a] Huichao He,[b] Bing Huang,[a] Yousong Liu,[a] Yong Zhou,*[bc] and Guangcheng Yang*[a]

[a]*Institute of Chemical Materials, China Academy of Engineering Physics, Mianyang 621900, China. E-mail: ygcheng@caep.cn*

[b]*State Key Laboratory of Environmental Friendly Energy Materials, School of Materials Science and Engineering, Southwest University of Science and Technology, Mianyang 621010, Sichuan, P. R. China. E-mail: zhouyong1999@nju.edu.cn*

[c]*School of Physics, Nanjing University, Nanjing 211102, Jiangshu, P. R. China.*

[+]*These authors contributed equally to this work.*

Section S1: Calculation of the electrochemical capacitance:

For three electrode cells, the specific capacitance of electrodes (C_m) were calculated with the previously reported methods [1, 2]:

(1) From GCD test by

$C_m = It/\Delta EM$,

where I, M, t and ΔE are the constant current (A), mass of the active material (g) of the electrode, the discharge time (s) and the voltage window (V), respectively.

(2) From CV text by

$C_m = S/2Mv\Delta E$,

where S, M, v and ΔE are the loop area, mass of the active material (mg) of the electrode, the scan rate (mV/s) and the voltage window (V), respectively.

For symmetrical cell, the specific capacitance of electrodes (C_m) were calculated from GCD test by $C_m = 2It/\Delta EM$, where M is the active materials of both electrodes and 2 results from serial connection of two identical capacitors.

The energy density (E) and power density (P) of the symmetrical SCs is obtained with

$E = C_m \Delta E^2 / 4*3600$,

$P = 3,600 * E / t$,

$C_m = 2It/\Delta EM$,

from GCD test, where t is the discharge time, ΔE represents the potential window, M represent the mass of the two electrodes.

Section S2: Calculation of the fraction of sp^2 bonding

First, the background of the carbon K-edge spectra caused by the tails of the plasmon peak(s) and other core - loss edges were removed by fitting the pre-edge region with a power law:

$I_{BG} = A * E^{-r}$

and then determining A and r and extrapolating it to the carbon K-edge region.

Second, the carbon K-edge spectra after removal of the background were normalized by the intensity at about 298 eV and were aligned at the π* peak (285.5 eV) for energy calibration [3].

Third, the fraction of sp^2 bonding was then calculated using the quantitative technique of Berger et al. [4] with reference to graphite (100%).

Table S1. Summarization of N concentration (atomic percent of nitrogen with respect to carbon and nitrogen) and ratios of N-6, N-5 and N-Q to the total N in the corresponding materials.

Materials	N content (N/(N+C) (%)	Ratio of N-6 (%)	Ratio of N-5 (%)	Ratio of N-Q (%)
NTC-650	19.0	68.98	20.75	10.27
NTC-700	14.3	69.12	18.4	12.47
NTC-750	11.7	60.16	14.7	25.13
NTC-800	10.3	59.84	13.4	26.72
NTC-1000	3.4	31.31	6.50	62.19

Table S2. Summarization of the N content and N-6 ratio for hollow carbons materails, N doped carbon nanotubes (N-CNT) and N doped graphene and other type of carbon materials ever reported in previous literatures.

Materials		Method	N content	Ratio of N-6 to total N content	Application	Specific capacitance	Ref.
Hollow carbons	NTC arrays	PVD and carbonization	14.3% (700 deg)	69.12%	supercapacitors	310.7 F g^{-1}	This work
	Nitrogen-Doped hollow spheres	hard template	7.92%	<50%	Li-S batteries & supercapacitors	201 F g^{-1}	Nature Communications 2015, **6**, 7221.
	Nitrogen-Doped hollow spheres	hard template	1.61%	<50%	Li-S batteries		Adv. Energy Mater. 2015, 1402263
	microporous hollow carbon	hard template	5.2%	44.2%	Li-S batteries		Adv. Funct. Mater. **2007**, *17*, 1828–1836
	hollow carbon arrays	hard template	3.8%	<50%	-		Carbon 2015, **83**, 275-281.
	Nitrogen doped carbon nanocapsules	hard template	7.1%	27.6%	ORR		Chemical Communications 2011, **47**, 4463-4465.
	Nitrogen-Doped Carbon Nanotubes	carbonization of polypyrrole	4.56%	<50%	supercapacitors	210 F g^{-1}	Chemistry–A European Journal 2013, **19**, 12306.
	N doped hollow microspheres	hard template	9.63%	16.8%	Li ion batteries		ACS Appl. Mater. Interfaces 2014, **6**, 19082
	N-doped hollow carbon microspheres	carbonization	9.08%	<50%	Li-S batteries		J. Mater. Chem. A, 2016, **4**, 15612
	N-doped Hollow Mesoporous Carbon	hard template	4.05%	<30%	Dye-Sensitized Solar Cells		J. Phys. Chem. C 2014, **118**, 16694
	nitrogen-doped carbon nanocages	hard template CVD	9.7% (700deg)	30.9%	ORR		Adv. Mater. 2012, **24**, 5593–5597
N-CNTs	N-CNTs	CVD	0.85%	35%			Carbon 2013, **52**, 316-325.
	N-CNTs	CVD	8.4%	~24%			Carbon 2010, **48**, 1498-1507.
	N-CNTs	CVD	1.5-5.1%	33-21.5%	supercapacitors	18 F g^{-1}	Phys. Status Solidi B 2013, **250**, 2586
	N-CNTs	CVD	3.6%	33.7%			Journal of Materials Science 2017, **52**, 10751-10765.
	N-CNTs	CVD	6%	<50%			J. Phys. Chem. C 2013, **117**, 7811-7817
N doped graphene	N doped graphene	chemical etching	3.5%	~50%			Nanotechnology 2016, **27**, 055404
	N doped graphene	CVD post doping	6.5%	63.1%	ORR		ACS Appl. Mater. Interfaces 2015, **7**, 14763−14769
	N doped graphene	CVD post doping	12.2%	90.4%	ORR		Adv. Funct. Mater. 2016, **26**, 5708–5717
	N doped graphene	plasma process	1.68-2.51%	30-52%	supercapacitors	280 F g^{-1}	Nano Lett. 2011, **11**, 2472–2477
	N doped oxide graphene	hydro-thermal reaction	10.0%	38.8%	supercapacitors	217 F g^{-1}	Nanoscale Research Letters 2015, **10**, 332
	N doped graphene	CVD	7.3-8.5%	10.4-26.1%	-		Scientific Reports 2016, **6**, 28330.
	N doped graphene oxide	hydrothermal	6.56%	28.2%	ORR		International Journal of Hydrogen Energy 2017, **42**, 28298
other carbon materials	N doped mesoporous carbon	soft-templating hydrothermal approach	14.5%	50.7%	supercapacitors	212 F g^{-1}	J. Mater. Chem. A, 2014, **2,** 11753
	N-doped carbon film	sputtering	12%	78%	-		Chemical Communications 2014, **50**, 557-559.
	N doped porous carbon	KOH activation in ammonia	7.5%–7.8%	13.5%	Li-ion storage		Adv. Mater. **2017**, 1603414
	few-layer carbon	CVD	8.2-11.9%	37.7-74.3%	supercapacitors	855 F g^{-1}	Science 2015, **350**, 1508.
	N-doped carbon film	sputtering	12%	78%			Chemical Communications 2014, **50**, 557-559.
	nitrogen-doped porous carbon	Carbonization	4.22%	37.2%	supercapacitors	450 F g^{-1}	J. Solid State Electrochem. 2015, **19**, 3087
	N doped porous Carbon	solvation volatilization/KOH activation	10.59%	30.2%	supercapacitors	220 F g^{-1}	ChemElectroChem 2017, **4**, 1–9
	Carbon Nanogears	hydrothermal + carbonization	~26%	67.3%	Li-ion storage		Adv. Energy Mater. 2016, **6**, 1600917

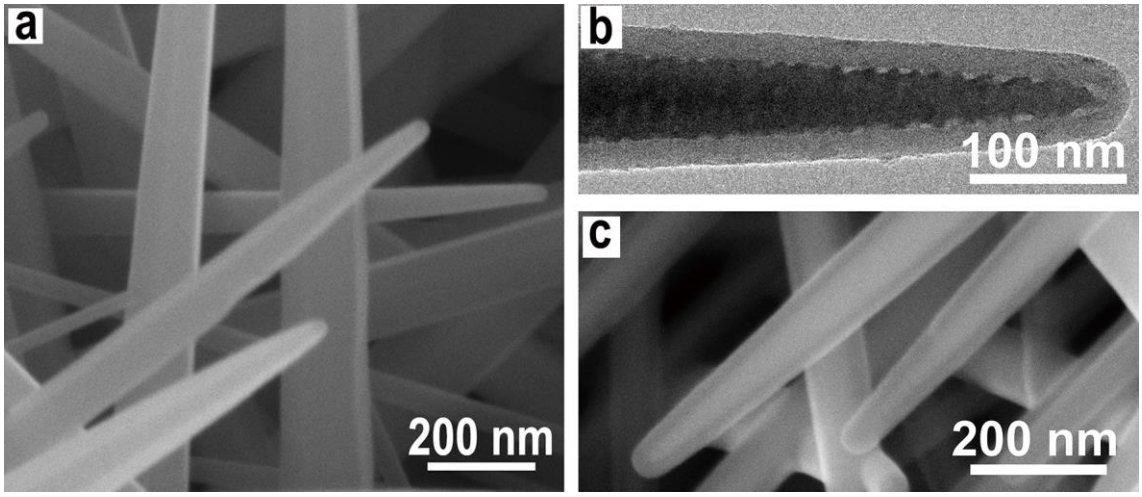

Figure S1. SEM (a) image of ZnO NWs. TEM (b) and SEM (c) image of the sample at 380 ^{o}C during temperature rising process.

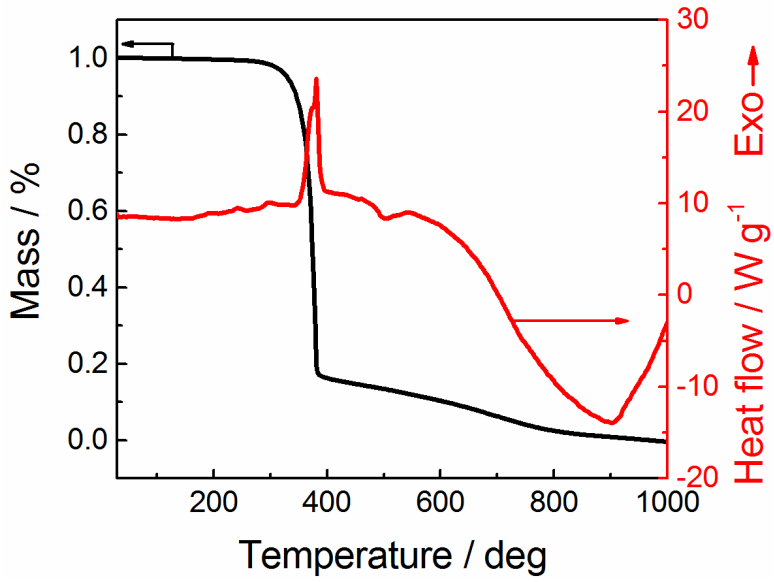

Figure S2. TGA and DSC curves of TATB during thermal degradation. Sample mass: 3.7 mg; Atmosphere: N_2; heating rate: 10 ^{o}C/min.

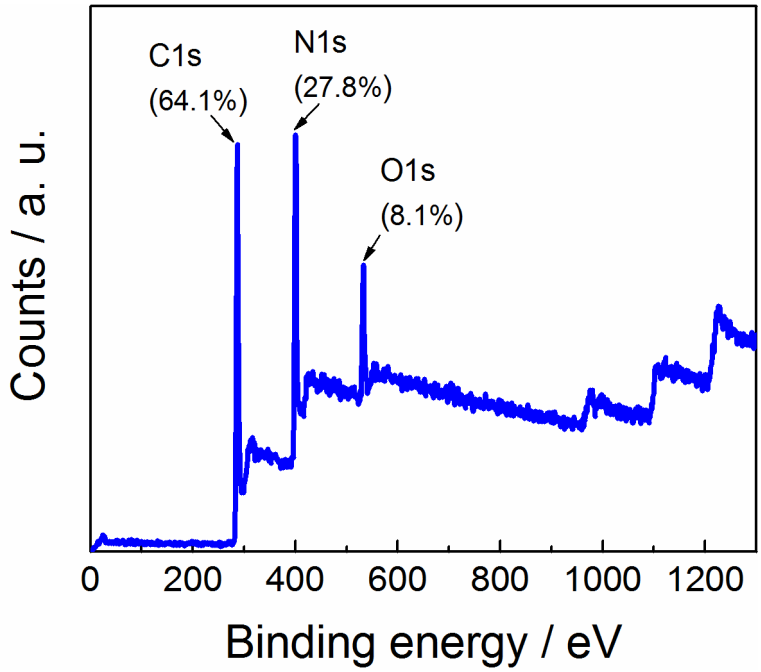

Figure S3. XPS of TATB after heating at 380 ^{o}C in N_2 atmosphere.

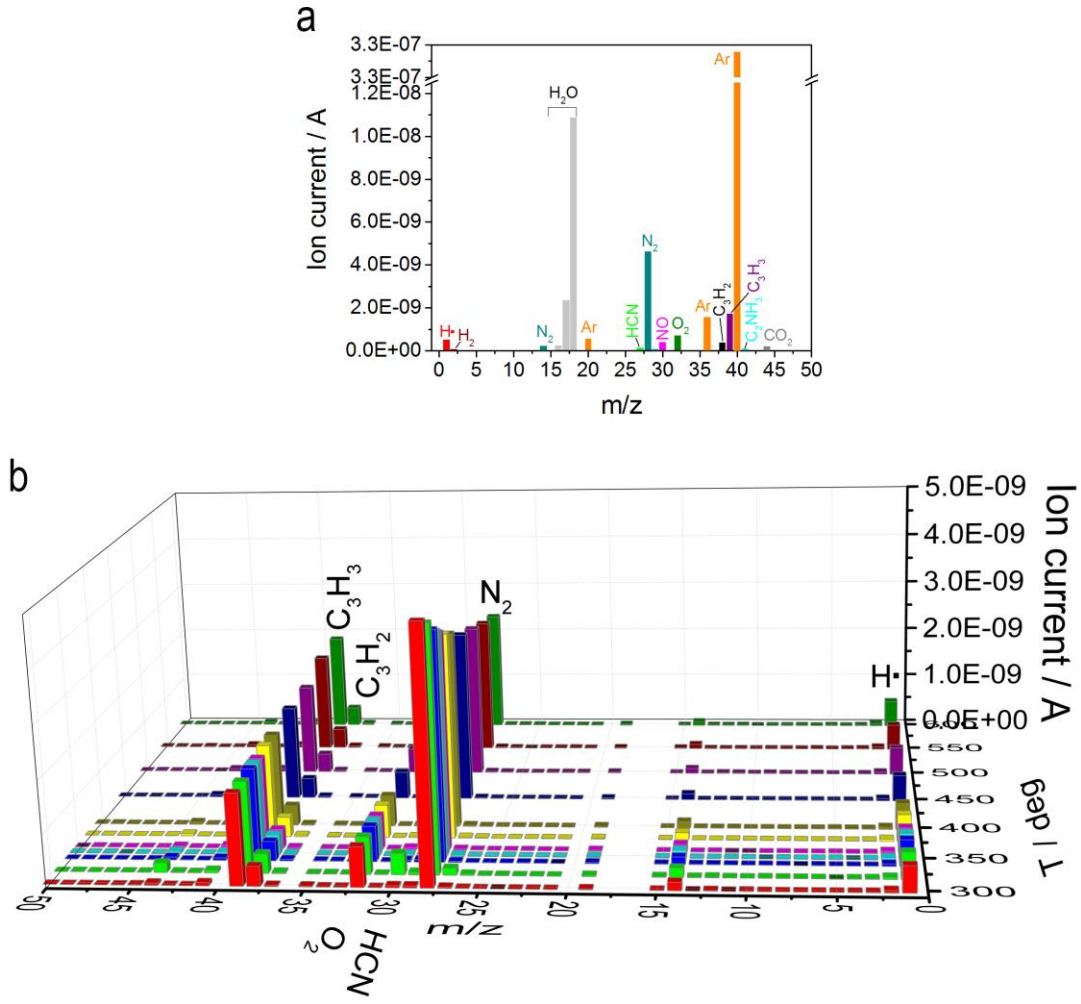

Figure S4. (a) Mass Spectrum showing the thermal decomposition products of TATB at 320 ^{o}C. (b) Variation of the thermal decomposition products of TATB with temperature.

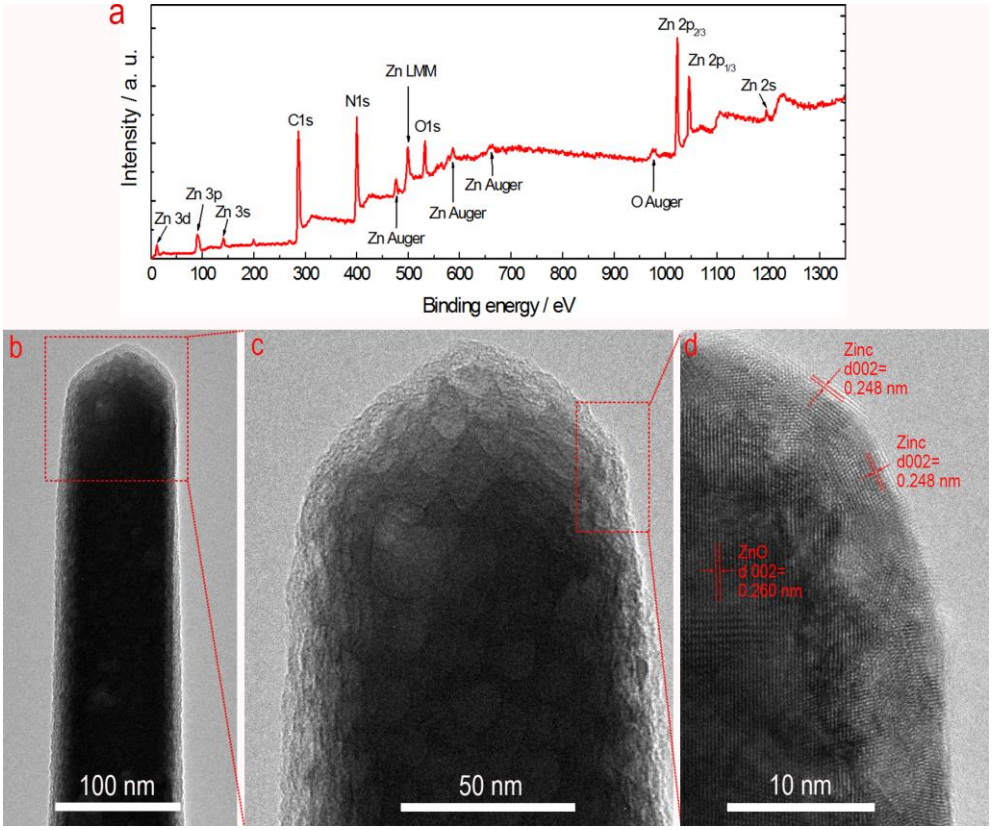

Figure S5. A designed confirmatory experiment demonstrated the reduction of ZnO to Zinc by the highly active thermal decomposition products of TATB. Experiment details: A piece of CC-ZnO was heated in a tube furnace with TATB powder as source under the flow of high-purity N_2 at 410 ^oC for 1 h. (a) XPS shows the elementals in the sample; (b) and (c) TEM images show the presence of an amorphous layer on ZnO NW; (d) High resolution TEM image shows the existence of nanocrystalline Zinc under electron beam irradiation during the HRTEM measurement.

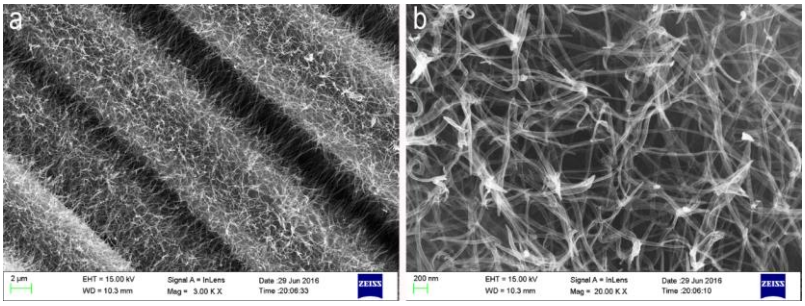

Figure S6. The NHCNWs synthesized under pure N_2 atmosphere using TATB as the only source and ZnO NWs as self-sacrificial templates at 700 ^{o}C for 1h with a heating rate of 3 ^{o}C/min. This result demonstrates that the ZnO templates can be removed by the decomposition products of TATB without H_2 within the atmosphere.

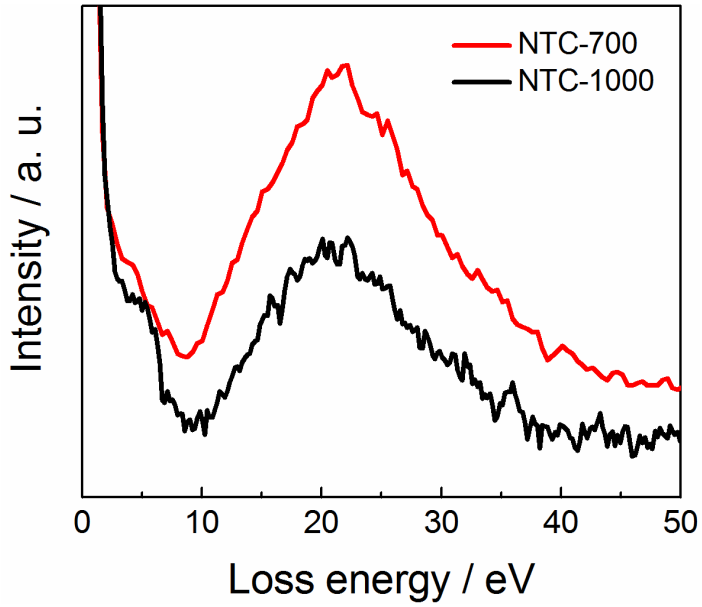

Figure S7. Electron energy-loss spectra in low-loss region from NTC-700 and NTC-1000.

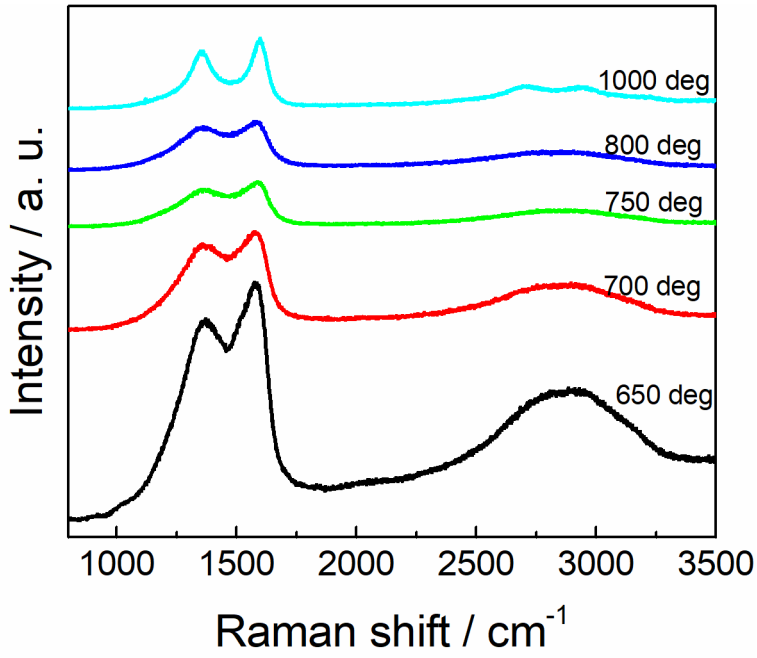

Figure S8. Raman scattering spectroscopy of the NTCs carbonized at different temperature. For Raman scattering spectroscopy test, the NTCs were take off from the carbon cloth by ultrasonic treatment of the samples immersed in ethanol. A NTCs film was fabricated on quartz glass substrate by diping coating of the above suspension of NTCs.

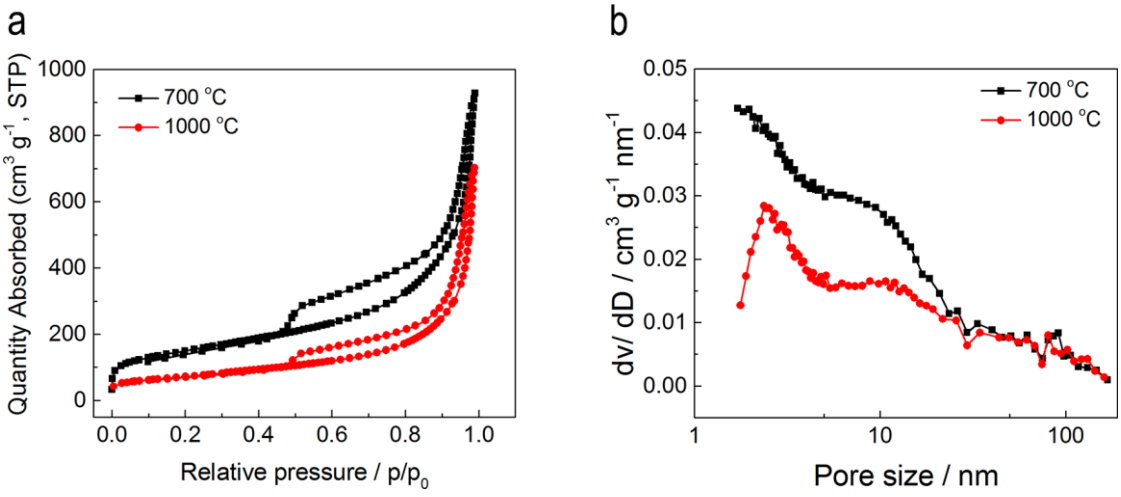

Figure S9. (a) N_2 adsorption/desorption isotherms and (b) pore-size distribution curves of the NTC-700 and NTC-1000.

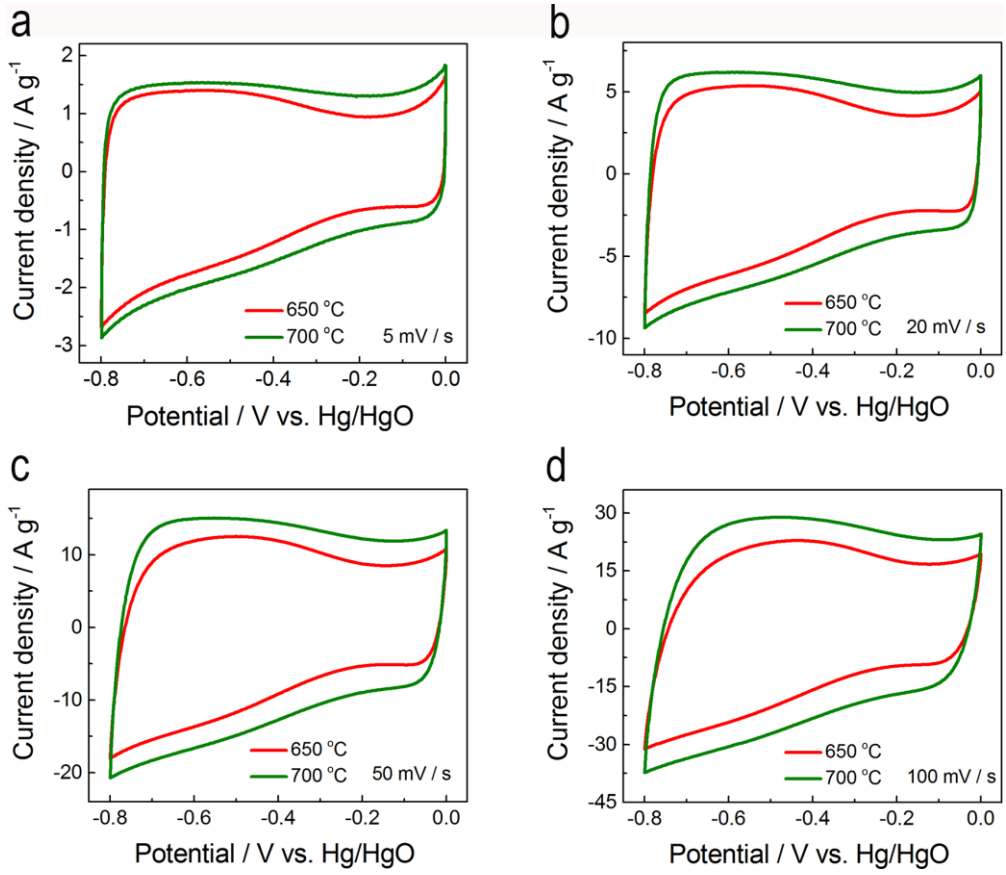

Figure S10. CV curves of the cells with NTC-650 and NTC-700 as working electrodes at different scan rates: (a) 5 mV/s; (b) 20 mV/s; (c) 50 mV/s and (d) 100 mV/s.

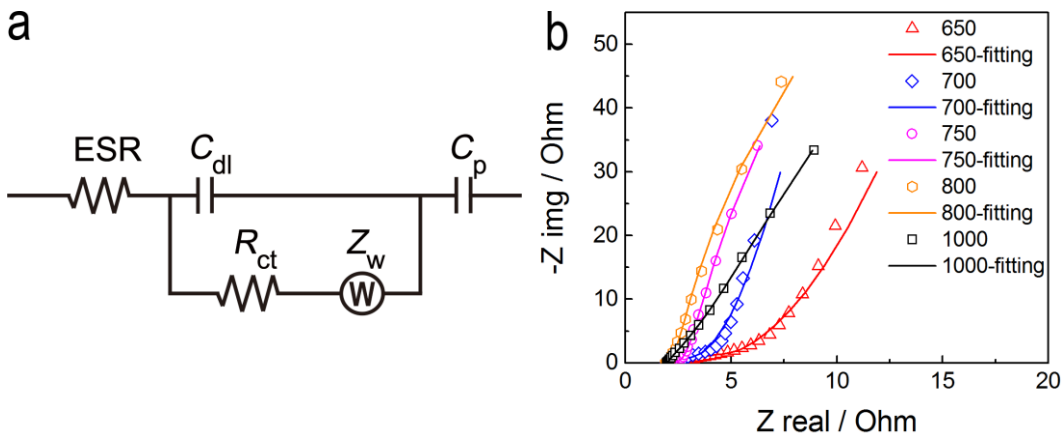

Figure S11. (a) Equivalent circuit used for fitting the EIS data, which comprised of equivalent series resistance (ESR), charge transport resistance (R_{ct}), EDL capacitance (C_{dl}), Warburg impedance (Z_w), and pseudocapacitance (C_p). (b) Nyquist plot of the electrode materials carbonized at different temperatures and the corresponding fitting curves obtained with the ZSimDemo version 3.30 d software (EChem Software, Ann Arbor, MI, USA).

Table S3. The fitted parameters of the Nyquist plots of NTC-650, NTC-700, NTC-750, NTC-800 and NTC-1000 using the equivalent circuit shown in Figure S10.

Circuit parameters	NTC-650	NTC-700	NTC-750	NTC-800	NTC-1000
R_s (ohm)	2.354	2.081	2.118	1.988	1.998
C_{dl} (F)	0.0002496	0.003453	0.006469	0.01665	0.01954
R_{ct} (ohm)	1.134	0.9913	0.1814	0.003826	0.001544
C_p (F)	0.0578	0.06232	0.05063	0.03981	0.03767
Z_w (Ω $s^{-0.5}$)	0.07162	0.2046	0.3771	0.3292	0.05159

Table S4. A comparison of the major characteristics of our results with some typical published data on carbon based SCs, including the specific capacitance (C_m (F g^{-1})/the corresponding charge-discharge current density (I_{CD} (A g^{-1}), the C_m retention (%) /the corresponding I_{CD} increase times, Cycling retention ratio (%)/ the corresponding cycling number and nitrogen content (%).

Materials	C_m (F g^{-1}) / I_{CD} (A g^{-1})	C_m retention (%) / I_{CD} increase times	Cycling retention (%)/ cycling number	N content (%)	Ref. No.
CC-NHCNW-700	310.7 / 0.8	93.6 / 10; 74.2 / 50	106.7 / 20, 000	14.3	This work
N doped hollow carbon nanospheres	203 / 0.1	88.6 / 10	95 / 5, 000	2.55	[5]
N doped hollow carbon nanospheres	240 / 1	72 / 10; 69 / 40	97.0 / 5,000	2.0	[6]
N doped hollow carbon spheres	213 / 0.5	61.6 / 10; 55.6 / 20	91 / 5,000	6.7	[7]
N doped hollow carbon spheres	230 / 0.5	78.2 / 10; 67.4 / 20	98 / 1,500	4.73	[8]
N doped hollow carbon spheres	266.9 / 0.5	86.17 / 10; 84 / 40	~100 / 1,000	7.4	[9]
N doped carbon nanotube	210 / 0.5	74.4 / 10	99 / 5,000	4.56	[10]
Hollow Carbon Nanococoons	220.0 / 0.5[a]	86.4 / 20	98 / 1,000	0	[11]
N doped porous carbon nanofibers	202 / 1	86 / 10; 81.7 / 30	97 / 3,000	7.22	[12]
N-doped carbon nanofiber	223.8 / 0.5	84.4 / 10; 78.5 / 100	106 / 20,000	--	[13]
double-capillary carbon nanofibers	245 / 0.5	68 / 60	94 / 10, 000	0	[14]
N-containing carbons	300 / 0.1	76.6 / 40	--	4.4	[15]
N doped porous carbon	325 / 1	59 / 10; 44 / 40	90.2 / 5,000	4.22	[16]
N doped porous carbon	340 / -	-	76.4 / 10, 000	6.0	[17]
N doped porous carbon	240 / 0.5[a]	-	98.7 / 3,000	2.2	[18]
Porous carbon nanosheets	257 / 0.5	71.6 / 100	98 / 2,000	0	[19]
Holey graphene frameworks	310 / 1	92.7 / 10	95 / 20,000	0	[20]
N doped graphene sheets	217 / 1	74 / 5	82.1 / 500	0	[21]

[a] mV s^{-1}

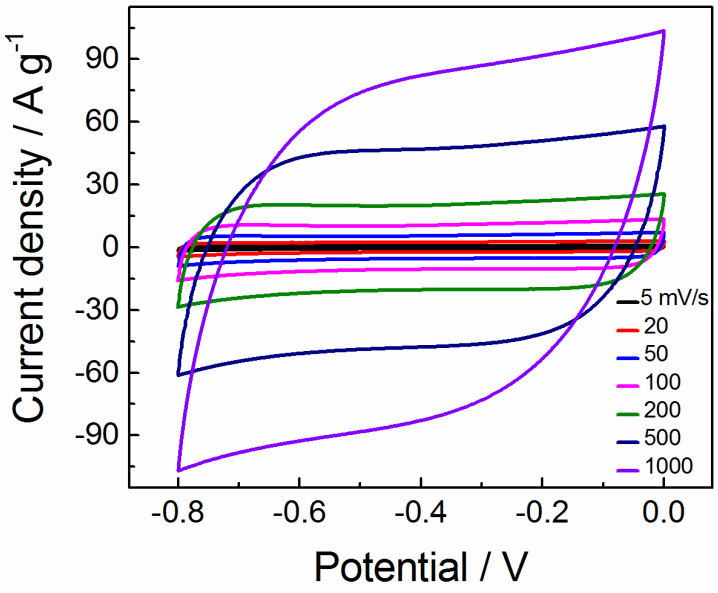

Figure S12. CV curves of a symmetric cell using NTC-700 at various scan rates.

References

[1] L. Liu, Y. Yu, C. Yan, K. Li, Z. Zheng, Wearable energy-dense and power-dense supercapacitor yarns enabled by scalable graphene-metallic textile composite electrodes, Nat. Commun., 6 (2015) 7260.

[2] T. Lin, I.-W. Chen, F. Liu, C. Yang, H. Bi, F. Xu, F. Huang, Nitrogen-doped mesoporous carbon of extraordinary capacitance for electrochemical energy storage, Science, 350 (2015) 1508-1513.

[3] Y. Murooka, N. Tanaka, S. Hirono, M. Hibino, Electron Energy-Loss Spectroscopy of Carbon Films Prepared by Electron-Cyclotron-Resonance Plasma Sputtering, Mater. Trans., 43 (2002) 2092-2096.

[4] S.D. Berger, D.R. McKenzie, P.J. Martin, EELS analysis of vacuum arc-deposited diamond-like films, Philos. Mag. Lett., 57 (1988) 285-290.

[5] F. Xu, Z. Tang, S. Huang, L. Chen, Y. Liang, W. Mai, H. Zhong, R. Fu, D. Wu, Facile synthesis of ultrahigh-surface-area hollow carbon nanospheres for enhanced adsorption and energy storage, Nat. Commun., 6 (2015) 7221.

[6] C. Liu, J. Wang, J. Li, M. Zeng, R. Luo, J. Shen, X. Sun, W. Han, L. Wang, Synthesis of N-Doped Hollow-Structured Mesoporous Carbon Nanospheres for High-Performance Supercapacitors, ACS Appl. Mater. Interfaces, 8 (2016) 7194-7204.

[7] J. Han, G. Xu, B. Ding, J. Pan, H. Dou, D.R. MacFarlane, Porous nitrogen-doped hollow carbon spheres derived from polyaniline for high performance supercapacitors, J. Mater. Chem. A, 2 (2014) 5352-5357.

[8] X. Liu, L. Zhou, Y. Zhao, L. Bian, X. Feng, Q. Pu, Hollow, Spherical Nitrogen-Rich Porous Carbon Shells Obtained from a Porous Organic Framework for the Supercapacitor, ACS Appl. Mater. Interfaces, 5 (2013) 10280-10287.

[9] H. Sun, Y. Zhu, B. Yang, Y. Wang, Y. Wu, J. Du, Template-free fabrication of nitrogen-doped hollow carbon spheres for high-performance supercapacitors based on a scalable homopolymer vesicle, J. Mater. Chem. A, 4 (2016) 12088-12097.

[10] G. Xu, B. Ding, P. Nie, L. Shen, J. Wang, X. Zhang, Porous Nitrogen-Doped Carbon Nanotubes Derived from Tubular Polypyrrole for Energy-Storage Applications, Chem. Eur. J., 19 (2013) 12306-12312.

[11] J. Zhang, K. Wang, S. Guo, S. Wang, Z. Liang, Z. Chen, J. Fu, Q. Xu, One-Step Carbonization Synthesis of Hollow Carbon Nanococoons with Multimodal Pores and Their Enhanced Electrochemical Performance for Supercapacitors, ACS Appl. Mater. Interfaces, 6 (2014) 2192-2198.

[12] L.-F. Chen, X.-D. Zhang, H.-W. Liang, M. Kong, Q.-F. Guan, P. Chen, Z.-Y. Wu, S.-H. Yu, Synthesis of Nitrogen-Doped Porous Carbon Nanofibers as an Efficient Electrode Material for Supercapacitors, ACS Nano, 6 (2012) 7092-7102.

[13] Y. Cheng, L. Huang, X. Xiao, B. Yao, L. Yuan, T. Li, Z. Hu, B. Wang, J. Wan, J. Zhou, Flexible and cross-linked N-doped carbon nanofiber network for high performance freestanding supercapacitor electrode, Nano Energy, 15 (2015) 66-74.

[14] J. Wang, J. Tang, Y. Xu, B. Ding, Z. Chang, Y. Wang, X. Hao, H. Dou, J.H. Kim, X. Zhang, Y. Yamauchi, Interface miscibility induced double-capillary carbon nanofibers for flexible electric double layer capacitors, Nano Energy, 28 (2016) 232-240.

[15] L. Zhao, L.-Z. Fan, M.-Q. Zhou, H. Guan, S. Qiao, M. Antonietti, M.-M. Titirici, Nitrogen-Containing Hydrothermal Carbons with Superior Performance in Supercapacitors, Adv. Mater., 22 (2010) 5202-5206.

[16] Y. Jiang, Y. Wang, Y. Zhang, X. Shu, Z. Chen, Y.-C. Wu, Controllable synthesis and capacitive performance of nitrogen-doped porous carbon from carboxymethyl chitosan by template carbonization method, J. Solid State Electrochem., 19 (2015) 3087-3096.

[17] C.O. Ania, V. Khomenko, E. Raymundo-Piñero, J.B. Parra, F. Béguin, The Large Electrochemical Capacitance of Microporous Doped Carbon Obtained by Using a Zeolite Template, Adv. Funct. Mater., 17 (2007) 1828-1836.
[18] F. Su, C.K. Poh, J.S. Chen, G. Xu, D. Wang, Q. Li, J. Lin, X.W. Lou, Nitrogen-containing microporous carbon nanospheres with improved capacitive properties, Energy Environ. Sci., 4 (2011) 717-724.
[19] X. Zheng, W. Lv, Y. Tao, J. Shao, C. Zhang, D. Liu, J. Luo, D.-W. Wang, Q.-H. Yang, Oriented and Interlinked Porous Carbon Nanosheets with an Extraordinary Capacitive Performance, Chem. Mater., 26 (2014) 6896-6903.
[20] Y. Xu, Z. Lin, X. Zhong, X. Huang, N.O. Weiss, Y. Huang, X. Duan, Holey graphene frameworks for highly efficient capacitive energy storage, Nat. Commun., 5 (2014) 4554.
[21] B. Xie, Y. Chen, M. Yu, X. Shen, H. Lei, T. Xie, Y. Zhang, Y. Wu, Carboxyl-Assisted Synthesis of Nitrogen-Doped Graphene Sheets for Supercapacitor Applications, Nanoscale Res. Lett., 10 (2015) 332.